# Wave-power extraction by a compact array of buoys

Xavier Garnaud, Chiang C. Mei

▶ **To cite this version:**

Xavier Garnaud, Chiang C. Mei. Wave-power extraction by a compact array of buoys. Journal of Fluid Mechanics, 2009, vol 635, pp 389-413. 10.1017/S0022112009007411 . hal-00674136

**HAL Id: hal-00674136**
**https://hal.science/hal-00674136**

Submitted on 25 Feb 2012

**HAL** is a multi-disciplinary open access archive for the deposit and dissemination of scientific research documents, whether they are published or not. The documents may come from teaching and research institutions in France or abroad, or from public or private research centers.

L'archive ouverte pluridisciplinaire **HAL**, est destinée au dépôt et à la diffusion de documents scientifiques de niveau recherche, publiés ou non, émanant des établissements d'enseignement et de recherche français ou étrangers, des laboratoires publics ou privés.

# Wave-power extraction by a compact array of buoys

XAVIER GARNAUD[1] † AND CHIANG C. MEI[2]

[1]Department of Aeronautics and Astronautics,
Massachusetts Institute of Technology
Cambridge, MA, 02139, USA

[2]Department of Civil and Environmental Engineering,
Massachusetts Institute of Technology
Cambridge, MA, 02139, USA

(Received 9 December 2009)

The majority of existing single-unit devices for extracting power from sea-waves relies on resonance at the peak frequency of the incident wave spectrum. Such designs usually call for structural dimensions not too small compared to a typical wavelength and yield high efficiency only within a limited frequency band. A recent innovation in Norway departs from this norm by gathering many small buoys in a compact array. Each buoy is too small to be resonated in typical sea conditions. In this article a theoretical study is performed to evaluate this new design. Within the framework of linearisation, we consider a periodic array of small buoys with similarly small separation compared to the typical wave length. The method of homogenization (multiple scales) is used to derive the equations governing the macro-scale behaviour of the entire array. These equations are then applied to energy extraction by an infinite strip of buoys, and by a circular array. In the latter case advantages are found when compared to a single buoy of equal volume.

## 1. Introduction

The prevailing ideas of wave-power extraction are based on matching the impedance of the extracting device to the characteristics of the incident wave. In particular for a single unit of an oscillating body, or for an oscillating water column, the device should be resonated at the peak frequency of the incoming wave and the extraction rate should equal that of the radiation damping. High efficiency is attainable in a limited frequency bandwidth around resonance. Ideas have been proposed to broaden the bandwidth by the method of phase control (Budal & Falnes (1980)) or by combining several devices of different impedances into one. Usually such devices must be sufficiently large to operate near the peak of the sea spectrum, and very small bodies can be resonated only at frequencies above the usual range of the energetic sea.

Recently Fred Olsen and ABB Power Systems Inc. (http://www02.abb.com) in Norway have designed a system called FO3 which consists of a rig with many small floating cylinders hanging underneath it. Energy is absorbed from the waves as they set the cylinders into vertical motion which then activates a hydraulic system driving a generator to produce electricity. Currently being tested is a 1:3-scale research model which measures

† Present address : Laboratoire d'Hydrodynamique – Ecole Polytechnique, 91128 Palaiseau, France

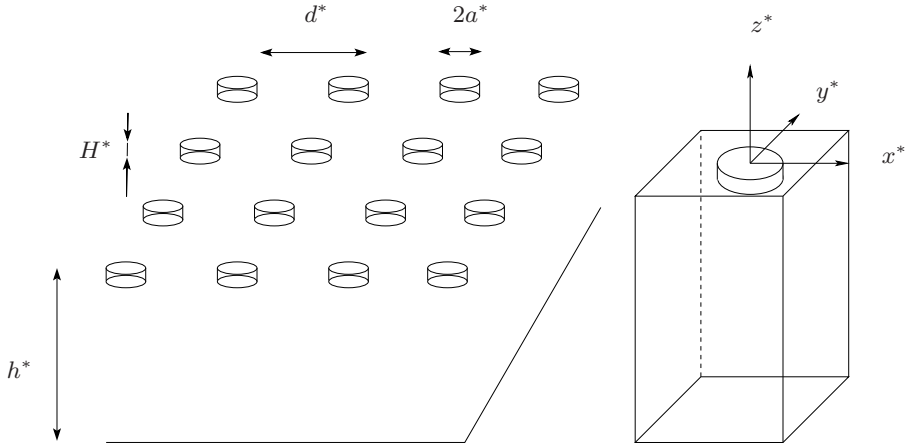


(a) A periodic array of buoys (b) Unit cell

FIGURE 1. Geometry of the array of buoys.

12 by 12 meters and is 8 meters high. It is estimated that the full-scale model can produce 2.52 MW from 6-meter high waves with a period of 9 seconds, comparable to the capacity of a wind turbine. Eventually a large array of many rigs can be installed over a large sea surface area and produce much more electricity.

In this paper we report a theoretical evaluation of this novel concept by examining a compact array of small buoys with spacings much shorter that the typical wavelength. Based on linearised theory of small amplitude waves we first employ the method of homogenization (i.e. multiple scales) to derive effective equations governing the dynamics on the macro-scale of the wave length. We show that for buoys of dimensions and spacing small compared to the water depth and wavelength, their presence and motion are manifest in a modified free surface condition on the wavelength scale. Explicit results are obtained for a long array of finite width attacked by normal incident sea, as well as a circular array of large radius. The dynamics and the energy efficiency are then compared with those of single buoys.

Specifically we shall consider a square array of small and identical buoys floating on the surface of the sea of constant mean depth $h^*$, as shown in figure 1. Each buoy is a vertical cylinder of circular cross section of radius $a^*$ and draft $H^*$, spaced at the distance $d^*$ from centre to centre. Assuming monochromatic waves of frequency $\omega^*$, the wave number $k^*$ of the incident waves is given by the real root of the dispersion relation

$$\omega^{*2} = gk^* \tanh(k^*h^*) \tag{1.1}$$

The incoming wave length and the sea depth are assumed to be comparable but both are much greater than the buoy radius $a^*$, the draft $H^*$ and the separation distance $d^*$. i.e.,

$$\frac{a^*}{h^*} \equiv \mu \ll 1, \qquad O(a^*) = O(H^*) = O(d^*), \qquad k^*h^* = O(1) \tag{1.2}$$

Wave energy is extracted from the heaving oscillation of each buoy through an absorbing device anchored to the seabed or attached to a fixed supporting structure.

## 2. Linearised governing equations

We employ the following symbols for physical domains: $\Omega_F$ is the fluid domain, $S_F$ is the free surface, $S_W$ is the lateral surface of the buoys, and $S_B$ is the bottom surface of the buoys. Let us denote all physical variables with asterisks. Assuming irrotational flow and infinitesimal waves, the velocity potential in water is governed by Laplace's equation

$$\Delta^*\Phi^* = \frac{\partial^2\Phi^*}{\partial {x^*}^2} + \frac{\partial^2\Phi^*}{\partial {y^*}^2} + \frac{\partial^2\Phi^*}{\partial {z^*}^2} = 0, \quad \boldsymbol{x}^* \in \Omega_F \tag{2.1}$$

The total pressure inside water is given by Bernoulli's equation:

$$p^* = -\rho\frac{\partial\Phi^*}{\partial t^*} - \rho g z^* \tag{2.2}$$

On the free surface $z^* = \eta^*(x^*, y^*, t^*)$, the kinematic boundary condition is

$$\frac{\partial\Phi^*}{\partial z^*} = \frac{\partial\eta^*}{\partial t^*}, \quad \boldsymbol{x}^* \in S_F \tag{2.3}$$

and the dynamic boundary condition is,

$$g\eta^* + \frac{\partial\Phi^*}{\partial t^*} = 0, \quad \boldsymbol{x}^* \in S_F \tag{2.4}$$

As the sea-surface pressure is assumed to be constant. On the sea bed the vertical velocity vanishes, which gives

$$\frac{\partial\Phi^*}{\partial z^*} = 0, \quad z^* = -h^* \tag{2.5}$$

On the side wall of the buoy, there is no normal velocity:

$$\frac{\partial\Phi^*}{\partial r^*} = 0, \quad \boldsymbol{x}^* \in S_W \tag{2.6}$$

where $r^*$ is the local radial coordinate from the axis of a cylindrical buoy. We assume that all buoys are installed on a large stationary frame or platform which is held fixed above the sea surface. On the flat bottom of the buoy the kinematic condition is

$$\frac{\partial\Phi^*}{\partial z^*} = \frac{\partial\zeta^*}{\partial t^*}, \quad \boldsymbol{x}^* \in S_B \tag{2.7}$$

where $\zeta^*(t^*)$ is the unknown vertical displacement of the buoy. Modelling the energy extraction device as a linear load force

$$-\lambda^*\frac{\partial\zeta^*}{\partial t^*} \tag{2.8}$$

on a moving buoy with a constant coefficient $\lambda^*$, the conservation law of vertical momentum of the buoy serves as the dynamic condition

$$M^*\frac{\partial^2\zeta^*}{\partial {t^*}^2} + \lambda^*\frac{\partial\zeta^*}{\partial t^*} + \pi {a^*}^2\rho g\zeta^* = -\rho\iint_{S_B}\frac{\partial\Phi^*}{\partial t^*}\,\mathrm{d}S^* \tag{2.9}$$

where $M^* = \rho\pi {a^*}^2 H^*$ is the buoy mass and $H^*$ its draft by Archimedis principle.

Let us introduce normalized variables as follows,

$$x_i^* = a^* x_i', \qquad t^* = t'\sqrt{\frac{h^*}{g}}, \qquad \Phi^* = A^*\sqrt{gh^*}\Phi, \qquad \eta^* = A^*\eta, \qquad \zeta^* = A^*\zeta \tag{2.10}$$

where $A^*$ is the amplitude of the incoming wave. Let us rewrite the governing equations.

Note that the length scale is the small radius of the buoy (the micro-scale). In normalized form, Laplace's equation (2.1) is unchanged. The free surface condition (2.3) becomes

$$\mu\frac{\partial\eta}{\partial t'}=\frac{\partial\Phi}{\partial z'},\quad \boldsymbol{x}'\in S_F \tag{2.11}$$

where

$$\mu=\frac{a^*}{h^*}\ll 1 \tag{2.12}$$

is the key parameter in this study. Equation (2.4) gives,

$$\eta+\frac{\partial\Phi}{\partial t'}=0,\quad \boldsymbol{x}'\in S_F \tag{2.13}$$

Equations (2.11) and (2.13) can be combined into

$$\frac{\partial\Phi}{\partial z'}+\mu\frac{\partial^2\Phi}{\partial t'^2}=0,\quad \boldsymbol{x}'\in S_F \tag{2.14}$$

and the condition on the seabed now reads

$$\frac{\partial\Phi}{\partial z'}=0,\quad z'=-\frac{h^*}{a^*}=-\frac{1}{\mu} \tag{2.15}$$

As $1/\mu\gg 1$, this micro-scale boundary condition is effectively applied at $z'\to-\infty$. On the buoy, the kinematic conditions are

$$\frac{\partial\Phi}{\partial r'}=0',\quad \boldsymbol{x}'\in S_W \tag{2.16}$$

and

$$\frac{\partial\Phi}{\partial z'}=\mu\frac{\partial\zeta}{\partial t'},\quad \boldsymbol{x}'\in S_B \tag{2.17}$$

The dynamic condition (2.9) now reads

$$\frac{a^*}{h^*}\frac{H^*}{a^*}\frac{\partial^2\zeta}{\partial t'^2}+\frac{\lambda^*\sqrt{g/h^*}}{\rho^* g\pi a^{*2}}\frac{\partial\zeta}{\partial t'}+\zeta=-\iint_{S_B}\frac{\partial\Phi}{\partial t'}\,\frac{\mathrm{d}S'}{\pi} \tag{2.18}$$

Defining

$$H'=\frac{H^*}{a^*}=O(1),\qquad\qquad \lambda=\frac{\lambda^*\sqrt{g/h^*}}{\rho^* g\pi a^{*2}}=O(1) \tag{2.19}$$

we change the same dynamic condition to dimensionless form,

$$\mu H'\frac{\partial^2\zeta}{\partial t'^2}+\lambda\frac{\partial\zeta}{\partial t'}+\zeta=-\frac{1}{\pi}\iint_{S_B}\frac{\partial\Phi}{\partial t'}\,\mathrm{d}S' \tag{2.20}$$

which can be combined with the kinematic condition (2.17) to give,

$$\left(\mu H'\frac{\partial^2}{\partial t'^2}+\lambda\frac{\partial}{\partial t'}+1\right)\frac{\partial\Phi}{\partial z'}=-\frac{\mu}{\pi}\iint_{S_B}\frac{\partial^2\Phi}{\partial t'^2}\,\mathrm{d}S' \tag{2.21}$$

## 3. Multiple-scale approximation

Our main objective is to consider the collective effects of many small buoys on the dynamics over a much larger region of dimensions comparable to the sea depth or to the wavelength. In view of the contrast of scales we seek an asymptotic approximation by the

method of multiple scales, and define the slow (macro-scale) coordinates without primes by

$$\boldsymbol{x} = \mu \boldsymbol{x}' \tag{3.1}$$

Let us denote by $\boldsymbol{\nabla}'$ and $\Delta'$ the gradient and Laplacian on the micro-scale and $\boldsymbol{\nabla}$ and $\Delta$ the corresponding operators on the macro-scale. We next introduce the expansions

$$\Phi = \mathrm{e}^{-\mathrm{i}\omega t'} \left[\phi_0(\boldsymbol{x}', \boldsymbol{x}) + \mu\phi_1(\boldsymbol{x}', \boldsymbol{x}) + \mu^2\phi_2\ (\boldsymbol{x}', \boldsymbol{x}) + \ldots\right] \tag{3.2}$$

$$\eta = \mathrm{e}^{-\mathrm{i}\omega t'} \left[\eta_0(x', y', x, y) + \mu\eta_1(x', y', x, y) + \mu^2\eta_2(x', y', x, y) + \ldots\right] \tag{3.3}$$

$$\zeta = \mathrm{e}^{-\mathrm{i}\omega t'} \left[\zeta_0(x', y', x, y) + \mu\eta_1(x', y', x, y) + \mu^2\zeta_2(x', y', x, y) + \ldots\right] \tag{3.4}$$

where $\omega$ is the dimensionless frequency normalized according to

$$\omega = \omega^* \sqrt{\frac{h^*}{g}} \tag{3.5}$$

Referring to the dimensionless governing equations in §1, we get from Laplace's equation,

$$\left(\Delta' + 2\mu\boldsymbol{\nabla}' \cdot \boldsymbol{\nabla} + \mu^2\Delta\right)(\phi_0 + \mu\phi_1 + ...) = 0, \quad \boldsymbol{x}' \in \Omega_F \tag{3.6}$$

The combined free surface condition becomes

$$\left(\frac{\partial}{\partial z'} + \mu\frac{\partial}{\partial z} - \mu\omega^2\right)(\phi_0 + \mu\phi_1 + ...) = 0, \quad \boldsymbol{x}' \in S_F \tag{3.7}$$

while the kinematic condition is

$$\left(\frac{\partial}{\partial z'} + \mu\frac{\partial}{\partial z} + \cdots\right)(\phi_0 + \mu\phi_1 + \mu^2\phi_2 + \cdots) = -\mathrm{i}\mu\omega(\eta_0 + \mu\eta_1 + \cdots), \quad \boldsymbol{x}' \in S_F \tag{3.8}$$

On the side wall of the buoy we have

$$\left(\frac{\partial}{\partial r'} + \mu\frac{\partial}{\partial r}\right)(\phi_0 + \mu\phi_1 + ...) = 0, \quad \boldsymbol{x}' \in S_W \tag{3.9}$$

and on the sea bed

$$\left(\frac{\partial}{\partial z'} + \mu\frac{\partial}{\partial z}\right)(\phi_0 + \mu\phi_1 + ...) = 0, \quad z' = -\frac{1}{\mu} \tag{3.10}$$

At the bottom of the buoy, the kinematic condition (2.17) gives

$$\left(\frac{\partial}{\partial z'} + \mu\frac{\partial}{\partial z}\right)(\phi_0 + \mu\phi_1 + \phi_2 + \cdots) = -\mathrm{i}\mu\omega(\zeta_0 + \mu\zeta_1 + \cdots), \quad z' = -H' \tag{3.11}$$

while the dynamic condition gives

$$\left(-\mu\omega^2 H' - \mathrm{i}\lambda\omega + 1\right)\left(\zeta_0 + \mu\zeta_1 + \mu^2\zeta_2 + \cdots\right) = \frac{\mathrm{i}\omega}{\pi} \iint_{S_B} (\phi_0 + \mu\phi_1 + \mu^2\phi_2 + \cdots)\,\mathrm{d}S' \tag{3.12}$$

From the combined buoy condition, we get

$$\left(-\mu\omega^2 H' - \mathrm{i}\lambda\omega + 1\right)\left[\frac{\partial\phi_0}{\partial z'} + \mu\left(\frac{\partial\phi_0}{\partial z} + \frac{\partial\phi_1}{\partial z'}\right) + \mu^2\left(\frac{\partial\phi_1}{\partial z} + \frac{\partial\phi_2}{\partial z'}\right) + \cdots\right] - \mu\frac{\omega^2}{\pi} \iint_{S_B} (\phi_0 + \mu\phi_1 + \mu^2\phi_2 + \cdots)\,\mathrm{d}S' = 0 \tag{3.13}$$

Let us also expand the factor

$$\frac{1}{1-\mathrm{i}\lambda\omega-\mu H'\omega^2}=\sum_{j=0}\mu^j\mathcal{F}_j(\omega) \tag{3.14}$$

where

$$\mathcal{F}_0(\omega)=\frac{1}{1-\mathrm{i}\lambda\omega},\quad \mathcal{F}_1(\omega)=\frac{H'\omega^2}{(1-\mathrm{i}\lambda\omega)^2},\quad \text{etc.} \tag{3.15}$$

By separating the orders, a series of micro-scale boundary value problems are then obtained at the orders $O(1), O(\mu)$ and $O(\mu^2)$.

### 3.1. *Leading order ($O(1)$)*

The governing conditions are homogeneous

$$\Delta'\phi_0=0, \qquad \boldsymbol{x}'\in\Omega \tag{3.16a}$$

$$\frac{\partial\phi_0}{\partial n'}=0, \qquad \boldsymbol{x}'\in S_F\cup S_W\cup S_B\cup S_b \tag{3.16b}$$

where $S_b$ denotes the sea bed at $z'=-\mu^{-1}\ll -1$. Let us define a unit cell of the array as shown in figure 1. Because there are a large number of periods in the array, we impose the condition that on the micro-scale, the solution is periodic, i.e.

$$\phi_0(x',y',z',\boldsymbol{x})=\phi_0(x'+d',y',z',\boldsymbol{x}) \tag{3.17a}$$

$$\phi_0(x',y',z',\boldsymbol{x})=\phi_0(x',y'+d',z',\boldsymbol{x}) \tag{3.17b}$$

with

$$d'\equiv d^*/a^* \tag{3.18}$$

being the centre-to-centre distance between adjacent buoys.

The leading-order solution is clearly independent of the micro-scale,

$$\phi_0=\phi_0(\boldsymbol{x}) \tag{3.19}$$

and the dependence on the macro-scale is yet to be found. It follows from (2.4) that

$$\eta_0=\mathrm{i}\omega\ \phi_0|_{z=0} \tag{3.20}$$

independently of the presence of the buoys. In the buoy-area (3.12) gives the buoy displacement

$$\zeta_0=\mathrm{i}\omega\mathcal{F}_0(\omega)\ \phi_0|_{z=0}\,,\quad \boldsymbol{x}\in\bar{S}_B. \tag{3.21}$$

Both $\eta_0$ and $\zeta_0$ are independent of the micro-scale coordinates, and they are related by

$$\zeta_0=\mathcal{F}_0\eta_0 \qquad \boldsymbol{x}'\in\bar{S}_B. \tag{3.22}$$

inside the buoy area.

### 3.2. *First order ($O(\mu)$)*

Using (3.19), we get from (3.6) that

$$\Delta'\phi_1=0,\quad \boldsymbol{x}'\in\Omega_F \tag{3.23a}$$

and from (3.7) that

$$\frac{\partial\phi_1}{\partial z'}=-\left(\frac{\partial\phi_0}{\partial z}-\omega^2\phi_0\right),\quad \boldsymbol{x}'\in S_F \tag{3.23b}$$

Equation (3.13) becomes

$$\frac{\partial \phi_1}{\partial z'} = -\left(\frac{\partial \phi_0}{\partial z} - \omega^2 \mathcal{F}_0 \phi_0\right), \quad \boldsymbol{x}' \in S_B \tag{3.23c}$$

We also have on the side wall of the buoy,

$$\frac{\partial \phi_1}{\partial r'} = -\frac{\partial \phi_0}{\partial r} = -n_i \frac{\partial \phi_0}{\partial x_i}, \quad \boldsymbol{x}' \in S_W \tag{3.23d}$$

where $\boldsymbol{n} = (n_1, n_2) = (\cos\theta, \sin\theta)$ denotes the unit vector normal to the side wall, and

$$\frac{\partial \phi_1}{\partial z'} = -\frac{\partial \phi_0}{\partial z}, \quad z' = -\frac{1}{\mu} \tag{3.23e}$$

on the seabed. In addition we require micro-scale periodicity on the cell boundaries. Once $\phi_1$ is found, $\zeta_1$ follows from (3.12). As it is usual in homogenization analysis, the macro-scale physics at the leading order is found by requiring the solvability of the inhomogeneous micro-scale problem at a higher order. The micro-scale cell problem for $\phi_1$ is inhomogeneous. By applying Gauss' theorem (or, equivalently applying Green's formula to $\phi_0$ and $\phi_1$ over a unit cell) $\phi_1$ over the cell volume, we get

$$\iint_{\partial\Omega} \frac{\partial \phi_1}{\partial n'} \, \mathrm{d}S' = 0 \tag{3.24}$$

where $\partial\Omega$ is the boundary of the cell. This is just the condition of solvability for the inhomogeneous problem of $\phi_1$. Since

$$\iint_{S_W} \frac{\partial \phi_1}{\partial r'} \, \mathrm{d}S' = -\mu \iint_{S_W} \frac{\partial \phi_0}{\partial r} \, \mathrm{d}S' = -\mu \boldsymbol{\nabla}\phi_0 \cdot \iint_{S_W} \boldsymbol{e}_r \, \mathrm{d}S' = 0 \tag{3.25}$$

we must have

$$\iint_{S_B} \frac{\partial \phi_1}{\partial z'} \, \mathrm{d}S' = -\iint_{S_F} \frac{\partial \phi_1}{\partial z'} \, \mathrm{d}S'$$

which gives at the leading order:

$$(1-f)\left(\frac{\partial \phi_0}{\partial z} - \omega^2 \phi_0\right) + f\left(\frac{\partial \phi_0}{\partial z} - \omega^2 \mathcal{F}_0 \phi_0\right) = 0, \quad z = 0 \tag{3.26}$$

where for circular buoys

$$f \equiv \frac{\pi a^{*2}}{d^{*2}} = \frac{\pi}{d'^2}, \quad \text{with} \quad 0 < f < \frac{\pi}{4} \tag{3.27}$$

is the area fraction of solid, or the *packing ratio*. Hence we have

$$\boxed{\frac{\partial \phi_0}{\partial z} - \omega^2 \left[1 + f(\mathcal{F}_0 - 1)\right] \phi_0 = 0, \quad z = 0, \quad \boldsymbol{x} \in \bar{S}_B.} \tag{3.28}$$

This is a key result of our approximation and gives the macro-scale boundary condition over the part of the mean sea surface covered by buoys. In the open water with no buoy, $f = 0$, (3.28) reduces to the familiar condition on the free surface:

$$\frac{\partial \phi_0}{\partial z} - \omega^2 \phi_0 = 0, \quad \boldsymbol{x} \in S_F \tag{3.29}$$

Because of (3.28), (3.23$b$) and (3.23$c$) can be rewritten as

$$\frac{\partial \phi_1}{\partial z'} = -\frac{\partial \phi_0}{\partial z}\left(1 - \frac{1}{1 - f(\mathcal{F}_0 - 1)}\right) \equiv -\beta \frac{\partial \phi_0}{\partial z}, \quad \boldsymbol{x} \in S_F \tag{3.30}$$

and

$$\frac{\partial \phi_1}{\partial z'} = -\frac{\partial \phi_0}{\partial z}\left(1 - \frac{\mathcal{F}_0}{1 + f(\mathcal{F}_0 - 1)}\right) \equiv -\beta' \frac{\partial \phi_0}{\partial z}, \quad \boldsymbol{x} \in S_B \tag{3.31}$$

which define $\beta$ and $\beta'$. In view of the forms of the boundary conditions, the solution of the micro-scale problem for $\phi_1$ in a unit cell can be sought in the form

$$\phi_1(\boldsymbol{x'}, \boldsymbol{x}) = -\sum_{j=1}^{3} N_j(\boldsymbol{x'}) \frac{\partial \phi_0}{\partial x_j} \tag{3.32}$$

Then the horizontal components $N_1, N_2$ are governed by the following boundary-value problems in the unit cell,

$$\Delta' N_j = 0, \qquad \boldsymbol{x'} \in \Omega_F \tag{3.33a}$$

$$\frac{\partial N_j}{\partial z'} = 0, \qquad \boldsymbol{x'} \in S_F \cup S_B \cup S_b \tag{3.33b}$$

$$\frac{\partial N_j}{\partial r'} = n_j, \qquad \boldsymbol{x'} \in S_W \tag{3.33c}$$

where the outerward normal to $S_W$ is $\boldsymbol{n} = (n_1, n_2, 0)$. The vertical component $N_3$ is governed instead by

$$\Delta' N_3 = 0, \qquad \boldsymbol{x'} \in \Omega_F \tag{3.34a}$$

$$\frac{\partial N_3}{\partial z'} = \beta, \qquad \boldsymbol{x'} \in S_F \tag{3.34b}$$

$$\frac{\partial N_3}{\partial z'} = 0, \qquad \boldsymbol{x'} \in S_b \tag{3.34c}$$

$$\frac{\partial N_3}{\partial z'} = \beta', \qquad \boldsymbol{x'} \in S_B \tag{3.34d}$$

$$\frac{\partial N_3}{\partial r'} = 0, \qquad \boldsymbol{x'} \in S_W \tag{3.34e}$$

The solutions are made unique by adding the constraint

$$\iiint_{\Omega_F} N_j(x)\, \mathrm{d}V' = 0, \quad j = 1, 2 \tag{3.35}$$

and $N_3 = 0$ at a point $\boldsymbol{x'} = \boldsymbol{x}'_b = (0, 0, -\mu^{-1})$ on the seabed. Being periodic in $(x', y')$, the harmonic functions $N_j(\boldsymbol{x'})$ are expected to diminish exponentially in $z'$. For confirmation we have performed a numerical simulation using Finite Elements. The results, given in figure 14 in Appendix A, show indeed that for a sufficiently slender cell the solutions $N_i$ are highly localized near the buoy. In view of (3.32), a consequence is that,

$$\frac{\partial \phi_1}{\partial z'} \to 0 \quad \text{as } z' \to -\infty \tag{3.36}$$

which in turn implies

$$\frac{\partial \phi_0}{\partial z} = 0, \quad z = -1 \tag{3.37}$$

because of (3.23$e$). This provides the seabed boundary condition for the macro-scale problem.

### 3.3. *Second order ($O(\mu^2)$) and the macro-scale problem*

At the second order the micro-scale problem for $\phi_2$ is again inhomogeneous,

$$\Delta'\phi_2 = -2\boldsymbol{\nabla}'\cdot\boldsymbol{\nabla}\phi_1 - \Delta\phi_0, \qquad \boldsymbol{x}'\in\Omega_F \tag{3.38a}$$

$$\frac{\partial\phi_2}{\partial z'} = -\left(\frac{\partial\phi_1}{\partial z}+\omega^2\phi_1\right), \qquad \boldsymbol{x}'\in S_F \tag{3.38b}$$

$$\frac{\partial\phi_2}{\partial z'} = -\left(\frac{\partial\phi_1}{\partial z}-\omega^2\mathcal{F}_0\phi_1-\omega^2\mathcal{F}_1\phi_0\right), \qquad \boldsymbol{x}'\in S_B \tag{3.38c}$$

$$\frac{\partial\phi_2}{\partial z'} = -\frac{\partial\phi_1}{\partial z}, \qquad z'=-\mu^{-1} \tag{3.38d}$$

$$\frac{\partial\phi_2}{\partial r'} = -\frac{\partial\phi_1}{\partial r}, \qquad \boldsymbol{x}'\in S_W \tag{3.38e}$$

As $|N_i|\to 0$ for $z'\to-\mu^{-1}$, (3.38$d$) reduces to :

$$\frac{\partial\phi_2}{\partial z'} = 0, \qquad z'=-\mu^{-1} \tag{3.39}$$

We now apply Green's formula for $\phi_0$ and $\phi_2$ in the unit cell and invoke their governing conditions on the micro-scale to get

$$\begin{aligned}\iiint_{\Omega_F}(\Delta\phi_0+2\boldsymbol{\nabla}'\cdot\boldsymbol{\nabla}\phi_1)\,\mathrm{d}V' &= \iint_{S_F}\left(\frac{\partial\phi_1}{\partial z}-\omega^2\phi_1\right)\mathrm{d}S' \\ &+\iint_{S_B}\left(\frac{\partial\phi_1}{\partial z}-\omega^2\mathcal{F}_0\phi_1-\omega^2\mathcal{F}_1\phi_0\right)\mathrm{d}S' - \iint_{S_W}\frac{\partial\phi_1}{\partial r}\,\mathrm{d}S'\end{aligned} \tag{3.40}$$

Using the fact that $\phi_1$ vanishes with $N_i$ outside the vertical distance of $O(1)$ from $z=0$, and that the cell volume $|\Omega_F|=O(1/\mu)$ is much greater than unity, we conclude that:

$$\iiint_{\Omega_F}\Delta\phi_0\,\mathrm{d}V' = 0$$

Because $\phi_0(\boldsymbol{x},t)$ is independent of $\boldsymbol{x}'$, we conclude that

$$\Delta\phi_0 = 0, \qquad -1<z<0 \tag{3.41}$$

Thus $\phi_0$ is harmonic on the macro-scale.

In summary, in the region with buoys, the macro-scale variation of $\phi_0(\boldsymbol{x})$ is governed by (3.41) in the fluid region, subject to the boundary condition (3.28) on $z=0$ in the buoy-covered area, and (3.37) on the seabed. In the open water without buoys, condition (3.28) must be replaced by (3.29), while (3.41) and (3.37) still apply. Note that due to the small draft $H'$, buoy inertia, hence resonance, is unimportant.

The homogenization analysis for finding the macro-scale behaviour can in principle be extended to periodic buoys of any shape. Once the macro-scale is completely determined, one can also derive the micro-scale fluctuations by solving the cell problems for the vector $\boldsymbol{N}(\boldsymbol{x}')$. Then $\phi_1(\boldsymbol{x},\boldsymbol{x}')$ can be found according to (3.32) and used to calculate wave forces on each buoy hence the individual apparent mass and radiation damping matrices. Such effort is needed for design, but is omitted here.

We shall now apply these macro-scale equations to examine wave power extraction from one- and two-dimensional arrays in response to a plane incident wave train arriving from $x\sim-\infty$.

## 4. Vertical eigenfunctions

As it is well known, the general solution in the open water region where $f = 0$ can be expressed as a series of the form

$$\phi_0(\boldsymbol{x}) = \sum_{n=0}^{\infty} \psi_n(x,y) f_n(z) \tag{4.1}$$

where

$$f_0 = c_0 \cosh(k_0(z+1)), \quad f_n = c_n \cos(\kappa_n(z+1)) \tag{4.2}$$

are real orthogonal eigenfunctions in $-1 < z < 0$, and $(k_0, k_1, \dots)$ are the eigenvalues of the dispersion relation,

$$\omega^2 = k_n \tanh(k_n), \quad n = 0, 1, \dots \tag{4.3}$$

In particular $k_0$ is the positive real root and $k_n \equiv \mathrm{i}\kappa_n$ is the n-th imaginary root i.e.,

$$\omega^2 = k_0 \tanh(k_0), \quad \omega^2 = -\kappa_n \tan(\kappa_n), \quad n = 1, 2, 3, \dots \tag{4.4}$$

With the choice of

$$c_0 = \sqrt{\frac{2}{1 + \omega^{-2}\sinh^2 k_0}}, \qquad c_n = \sqrt{\frac{2}{1 - \omega^{-2}\sin^2(\kappa_n)}} \tag{4.5}$$

the vertical eigenfunctions are orthonormal,

$$\langle f_n | f_m \rangle \equiv \int_{-1}^{0} f_n(z) f_m(z)\, \mathrm{d}z = \delta_{nm} \tag{4.6}$$

Furthermore the horizontal factors $\psi_n$ must satisfy Helmholtz equations in the horizontal plane

$$\left(\frac{\partial^2}{\partial x^2} + \frac{\partial^2}{\partial y^2} + k_0^2\right)\psi_0 = 0, \tag{4.7a}$$

$$\left(\frac{\partial^2}{\partial x^2} + \frac{\partial^2}{\partial y^2} - \kappa_n^2\right)\psi_n = 0, \quad n = 1, 2, 3, ... \tag{4.7b}$$

In the region of wave absorbing buoys we also assume

$$\phi_0(\boldsymbol{x}) = \sum_{n=0}^{\infty} \Psi_n(x,y) F_n(z) \tag{4.8}$$

It can be shown that the eigenfunctions $\{F_n\}$, $n = 0, 1, 2, \dots$ are the solutions of the boundary value problem

$$\begin{aligned} F_n''(z) - K_n^2 F_n(z) &= 0 \qquad -1 < z < 0 \\ \left(F_n' - \sigma^2 F_n\right) &= 0 \qquad z = 0 \\ F_n' &= 0, \qquad z = -1, \end{aligned} \tag{4.9}$$

where $\sigma$ is defined by

$$\sigma^2 \equiv \omega^2[f\mathcal{F}_0(\omega) + (1-f)] \tag{4.10}$$

and is complex due to energy extraction. Therefore the eigenfunctions $F_n$ are complex

$$F_n = C_n \cosh K_n(z+1) \tag{4.11}$$

The eigenvalue $K_n$ is the $n-$th complex root of the relation

$$\sigma^2 = K_n \tanh K_n \tag{4.12}$$

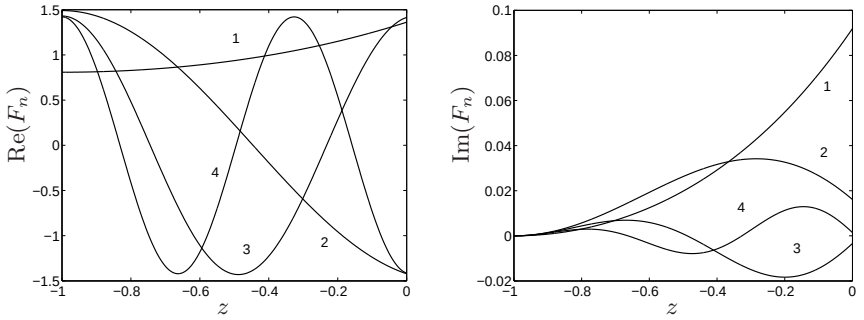


(a) Real part of eigenfunction $F_n$ with $n$ labelled next to the curves.

(b) Imaginary part of eigenfunction $F_n$ with $n$ labeled next to the curves.

FIGURE 2. First few vertical eigenfunctions in the buoy domain according to (4.9). For $\omega = 1$, $\lambda = 1$ and $f = 0.2$

This type of dispersion relation with complex $\sigma^2$ arises also for waves through a porous media and has been studied by Dalrymple *et al.* (1991) and McIver (1998).

It is straightforward to show that the set $\{F_n\}$ is orthogonal. By choosing the coefficients $\{C_n\}$ to be

$$C_n = \sqrt{\frac{2}{\sigma^{-2}\sinh^2(K_n) + 1}} \tag{4.13}$$

the eigenfunctions $\{F_n\}$ are also orthonormal,

$$\langle F_n | F_m \rangle \equiv \int_{-1}^{0} F_n(z) F_m(z) dz = \delta_{nm} \tag{4.14}$$

Since $K_n$ is complex, the square root above is defined such that if the complex radical is $z = re^{i\theta}$, its phase is limited to the range $-\pi < \theta \leq \pi$. Dalrymple *et al.* (1991); McIver (1998) showed that this set of functions is a complete basis provided the eigenvalues $K_n$ are distinct, which is in general the case.

For a given frequency $\omega$, packing ratio $f$ and damping rate $\lambda$, $\sigma$ is first defined. $K_n$ and $F_n$ are found numerically. Before employing an usual iterative algorithm to solve the complex transcendental equation, a good initial guess of the solution is needed. For this purpose we solved the eigenvalue problem governed by (4.9) by the numerical method of finite elements with a regular mesh and third-order Laplace elements. The resulting $K_n$'s are used as a initial guesses for further iteration of (4.12). Sample $F_n$'s are shown in figure 2. Sample eigenvalues are given in Table 1.

Note that for $f = 0$, $k$ is purely real and $k_n = i\kappa_n, n = 1, 2, 3...$ are purely imaginary. For $f \ll 1$, $K_0$ is almost real and $K_n, n = 1, 2, 3, ...$ are almost imaginary. Perturbation solutions of (4.12) have been used to confirm the values in Table 1 where $f = 0.2$.

We now apply these results to examine two simple arrays.

## 5. A long array of energy-absorbing buoys

Referring to figure 3, let us first consider a long array of width $L$ with its edges parallel to the crests of incoming plane waves. Assuming an incoming wave of unit amplitude, the velocity potential in the open water on the incidence side (zone I) is

$$\phi_I(x, z) = \frac{-i}{\omega f_0(0)} \left( e^{ik_0 x} f_0(z) + \sum_{n=0}^{\infty} R_n e^{-ik_n x} f_n(z) \right), \quad -\infty < x < 0 \tag{5.1}$$

| $K_n$ | $\omega = 0.5$ | $\omega = 1$ | $\omega = 2$ |
|---|---|---|---|
| $K_1$ | 0.5107 + 0.0230i | 1.1165 + 0.0835i | 3.3669 + 0.3159i |
| $K_2$ | 0.0067 + 3.0634i | 0.0357 + 2.8342i | 0.0545 + 2.1332i |
| $K_3$ | 0.0032 + 6.2448i | 0.0163 + 6.1376i | 0.0449 + 5.7538i |
| $K_4$ | 0.0021 + 9.3992i | 0.0107 + 9.3286i | 0.0322 + 9.0697i |
| $K_5$ | 0.0016 +12.5472i | 0.0080 +12.4945i | 0.0247 +12.2996i |
| $K_6$ | 0.0013 +15.6927i | 0.0064 +15.6505i | 0.0200 +15.4944i |
| $K_7$ | 0.0011 +18.8368i | 0.0053 +18.8017i | 0.0168 +18.6715i |
| $K_8$ | 0.0009 +21.9802i | 0.0046 +21.9502i | 0.0144 +21.8385i |
| $K_9$ | 0.0008 +25.1232i | 0.0040 +25.0969i | 0.0126 +24.9991i |
| $K_{10}$ | 0.0007 +28.2658i | 0.0035 +28.2425i | 0.0113 +28.1555i |

TABLE 1. First ten eigenvalues of (4.12) for $\lambda = 1$ and $f = 0.2$.

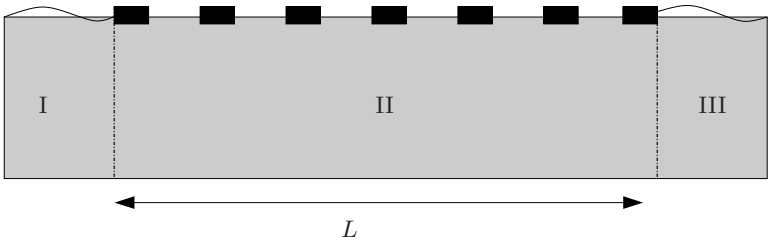


FIGURE 3. Cross section of an infinitely long array.

where $k_0$ is real and $k_n = \mathrm{i}\kappa_n, n = 1, 2, 3, ...$ are imaginary roots of the dispersion relation. In zone II of the buoys, the potential is

$$\phi_{II}(x,z) = \frac{-\mathrm{i}}{\omega f_0(0)} \sum_{n=0}^{\infty} \left( B_n \mathrm{e}^{\mathrm{i}K_n x} + B'_n \mathrm{e}^{-\mathrm{i}K_n x} \right) F_n(z), \quad 0 < x < L \tag{5.2}$$

and in the open water on the transmission side (zone III) we have

$$\phi_{III}(x,z) = \frac{-\mathrm{i}}{\omega f_0(0)} \sum_{n=0}^{\infty} T_n \mathrm{e}^{\mathrm{i}k_n x} f_n(z), \quad L < x < \infty \tag{5.3}$$

The eigenvalues $(k_n, K_n)$ and eigenfunctions $(f_n, F_n)$ have been defined in §4. Let us introduce

$$U(z) = \frac{\partial \phi_0}{\partial x}(0,z), \qquad U'(z) = \frac{\partial \phi_0}{\partial x}(L,z) \tag{5.4}$$

as the horizontal velocities at $x = 0$ and $x = L$ respectively. Requiring flux continuity and using the orthogonality of eigenfunctions, we find

$$R_0 = 1 - \frac{\langle U | f_0 \rangle}{\mathrm{i}k_0} \qquad R_n = -\frac{\langle U | f_n \rangle}{\mathrm{i}k_n} \tag{5.5a}$$

$$B_n = -\frac{\langle (U' - \mathrm{e}^{-\mathrm{i}K_n L} U) | F_n \rangle}{2K_n \sin(K_n L)} \qquad B'_n = -\frac{\langle (U' - \mathrm{e}^{\mathrm{i}K_n L} U) | F_n \rangle}{2K_n \sin(K_n L)} \tag{5.5b}$$

$$T_n = \frac{\langle U' | f_n \rangle}{\mathrm{i}k_n \mathrm{e}^{\mathrm{i}k_n L}} \tag{5.5c}$$

We further require continuity of pressure (i.e., of potentials) at $x = 0$

$$f_0(z) + \left(1 - \frac{\langle U|f_0\rangle}{\mathrm{i}k_0}\right) f_0(z) - \sum_{n\geq 1} \frac{\langle U|f_n\rangle}{\mathrm{i}k_n} f_n(z)$$
$$= -\sum_{n\geq 0} \frac{\langle (U' - \cos(K_n L)U)|F_n\rangle}{K_n \sin(K_n L)} F_n(z) \tag{5.6}$$

and at $x = L$

$$-\sum_{n\geq 0} \frac{\langle (U'\cos(K_n L) - U)|F_n\rangle}{K_n \sin(K_n L)} F_n(z) = \sum_{n\geq 0} \frac{\langle U'|f_n\rangle}{\mathrm{i}k_n} f_n(z) \tag{5.7}$$

These are a pair of integral equations for $U(z)$ and $U'(z)$ in $-1 < z < 0$. Let their solutions be represented by the following orthonormal expansions

$$U = \sum_m U_m F_m, \quad U' = \sum_m U'_m F_m, \quad -1 < z < 0 \tag{5.8}$$

with unknown coefficients, and let

$$f_n = \sum_m M_{nm} F_m \quad \text{where} \quad \langle f_n|F_m\rangle = M_{nm} \tag{5.9}$$

The matrix elements $M_{nm}$ can be obtained explicitly,

$$M_{nm} = \omega^2 f(1 - \mathcal{F}) \frac{c_n \cosh(k_n) C_m \cosh(K_m)}{(k_n^2 - K_m^2)} \tag{5.10}$$

Equations (5.6) and (5.7) become

$$2f_0(z) \sum_{n,q} M_{nq} U_q \frac{1}{\mathrm{i}k_n} f_n(z) = \sum_n \left(-\frac{U'_n}{K_n \sin(K_n L)} + \frac{U_n}{K_n \tan(K_n L)}\right) F_n(z) \tag{5.11}$$

$$\sum_{n,q} M_{nq} U'_q \frac{1}{\mathrm{i}k_n} f_n(z) = \sum_n \left(-\frac{U'_n}{K_n \tan(K_n L)} + \frac{U_n}{K_n \sin(K_n L)}\right) F_n(z) \tag{5.12}$$

By taking the scalar product with $F_p$ for $p = 0, 1, 2, 3, ...$ in turn we obtain from (5.11) and (5.12)

$$2M_{0p} - \sum_{n,q} M_{nq} U_q \frac{1}{\mathrm{i}k_n} M_{np} = \left(-\frac{1}{K_p \sin(K_p L)}_p U'_n + \frac{1}{K_p \tan(K_p L)} U_p\right) \tag{5.13}$$

and

$$\sum_{n,q} M_{nq} U'_q \frac{1}{\mathrm{i}k_n} M_{np} = \left(-\frac{1}{K_p \tan(K_p L)} U'_p + \frac{1}{K_p \sin(K_p L)} U_p\right) \tag{5.14}$$

The expansion coefficients $U_n, U'_q$ are solved numerically after truncation. Afterwards we get the buoy displacement $\zeta_0$ from the expression of $\phi_{II}$. The transmission and reflection coefficients follow from (5.5$c$) and (5.5$a$) :

$$T \equiv T_0 = \frac{M_{0q} U'_q}{\mathrm{i}k_0 \mathrm{e}^{\mathrm{i}k_0 L}} \tag{5.15}$$

and

$$R \equiv R_0 = 1 - \frac{\langle U|f_0\rangle}{\mathrm{i}k_0} \tag{5.16}$$

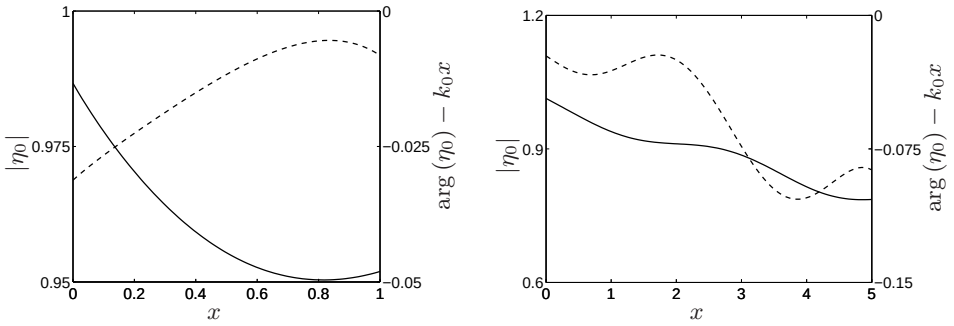


(a)$L = 1$ (b) $L = 5$

FIGURE 4. Free surface elevation inside an array of length $L = 1$ (a) and $L = 5$ (b). Solid curve: Amplitude. Dashed curve: Phase difference from the undisturbed plane wave, in radians. The parameters are $f = 0.2$, $\lambda = 0.5$ and $k_0 = 1$.

The dimensionless power-extraction efficiency is

$$\mathcal{E} = 1 - |T|^2 - |R|^2. \tag{5.17}$$

Figure 4 shows the amplitude and phase of the free surface elevation inside the buoy region for array width of $L = 1$ and $L = 5$ according the macro-scale normalization. The buoy displacement is simply proportional to that of the free surface displacement in the same region by the complex reduction factor $\mathcal{F}_0$ whose magnitude

$$|\mathcal{F}_0| = \frac{1}{\sqrt{1 + (\lambda\omega)^2}} \tag{5.18}$$

is smaller for higher extraction rate and frequency. Note first that there is no resonance. For a fixed width $L$, the reflection coefficient $R$ increases with the extraction rate $\lambda$, as shown in figure 5. Both the transmission coefficient $T$ and the extraction efficiency $\mathcal{E}$ reach optimal? maximum values for some intermediate extraction rate around $\lambda = 0.5$ as shown in figure 7(a). The precise optimal value is around 0.5 and can be determined numerically.

For a fixed extraction rate, the effects of array width $L$ on the transmission and reflection coefficients are shown in figure 6(b). The corresponding extraction efficiency is shown in figure 7(b). The oscillatory variation of the reflection coefficient shown in figures 5(b) and 6(b) is due to interference by strong reflection, similar to the case of a finite shelf (cf. Mei *et al.* (2005), p. 149). In the transmission coefficient, this oscillatory behaviour is less prominent due to energy extraction. We have indeed checked that in the limit of extremely strong load force, $\lambda \gg 1$, the buoys no longer move. In this case reflection is the strongest and the oscillatory variation in $T$ is recovered.

While it is not surprising that a larger $L$ gives a higher efficiency, as shown in figure 7(b), it is nevertheless interesting that the gain of energy extraction with a wider array is more significant at low frequency. In practical situations $k_0 = k_0^* h^*$ will likely be between 0 and 3. Our predictions can help the designer to choose the proper width by considering both efficiency and construction economy.

In general scattering is significant, hence the maximum efficiency of energy extraction is somewhat lower than that a large beam-sea device such as a Salter's duck (see Mynett, Serman & Mei (1979)).

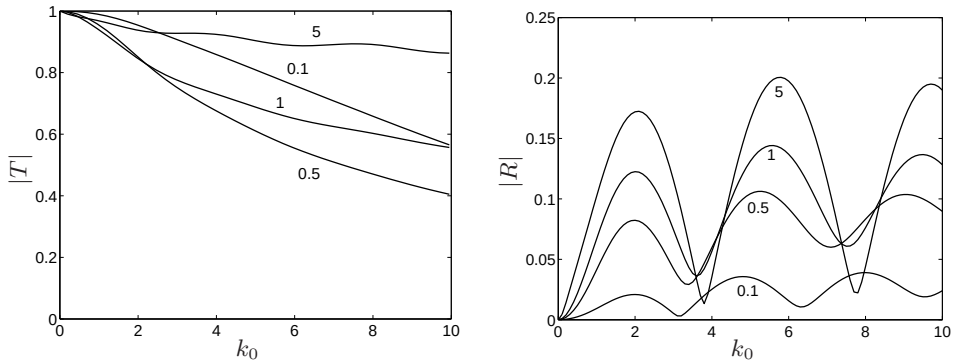


(a)Transmission coefficient. (b) Reflection coefficient.

FIGURE 5. Transmission and reflection coefficients for an array of buoys with various extraction rates $\lambda$, as indicated by numbers next to each curve. The packing ratio is $f = 0.2$ and $L = 1$.

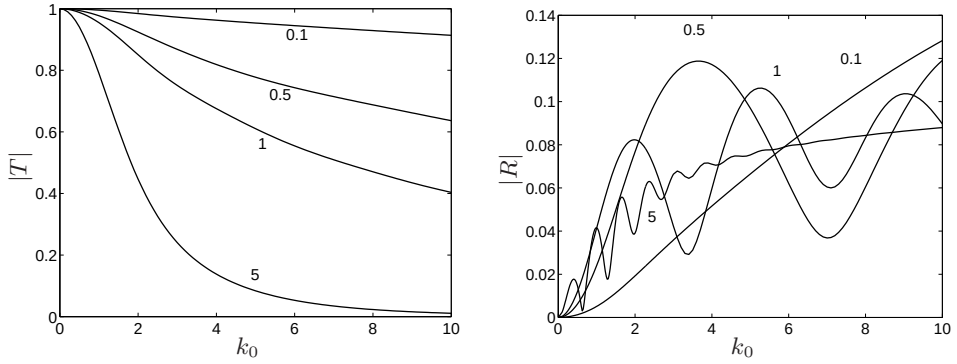


(a)Transmission coefficient. (b) Reflection coefficient.

FIGURE 6. Transmission and reflection coefficients for a buoy array with various array width $L$, as indicated next to each curve. The packing ratio is $f = 0.2$ and $\lambda = 0.5$

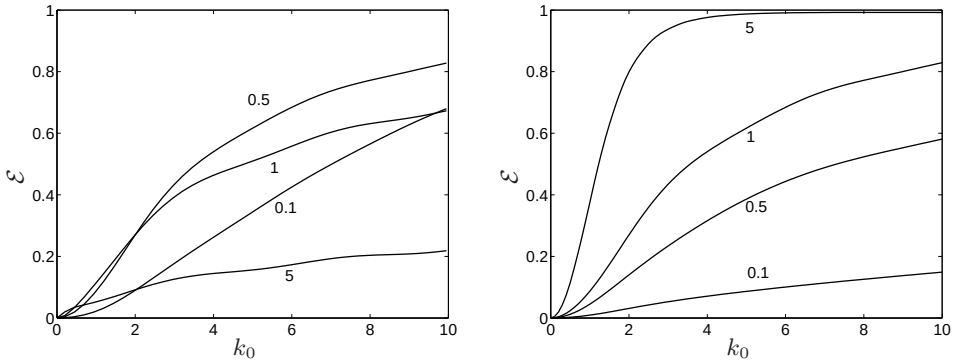


(a) Effects of extraction rate for $L = 1$. (b) Effects of total array width for $\lambda = 0.5$.

FIGURE 7. Variation of the extraction efficiency of a long array of finite width with (a) the extraction rate $\lambda$ for a given array width and (b) the array width $L$ for a given $\lambda$. Values of the varying parameter are indicated by numbers next to each curve. The packing ratio is $f = 0.2$.

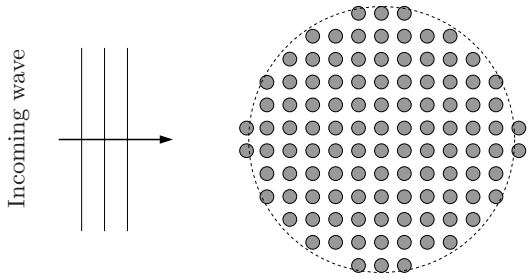


FIGURE 8. A circular array of energy-absorbing buoys.

## 6. A circular array

### 6.1. *The solution*

Now let many buoys be gathered inside a circular area of radius $R$. First, it is well known that the incident plane wave in the direction of $x$ can be expanded as a sum of partial waves (see e.g. Abramowitz & Stegun 1964)

$$\phi_i(\boldsymbol{x}) = \frac{-\mathrm{i}}{\omega f_0(0)} f_0(z) \mathrm{e}^{\mathrm{i}k_0 x} = \frac{-\mathrm{i}}{\omega f_0(0)} f_0(z) \sum_{m=0}^{\infty} \varepsilon_m \mathrm{i}^m J_m(k_0 r) \cos(m\theta)$$

where $\varepsilon_0 = 1$ and $\varepsilon_n = 2$ for $n = 1, 2, 3, \ldots$ are the Jacobi symbols. Let us express the total solution as

$$\phi = \sum_{m=0}^{\infty} \bar{\phi}_m(r, z) \cos(m\theta) \tag{6.1}$$

In the open water, the $m$-th mode potential $\bar{\phi}_m$ can be written as

$$\bar{\phi}_m = \frac{-\mathrm{i}}{\omega f_0(0)} \left( \varepsilon_m \mathrm{i}^m J_m(k_0 r) f_0(z) + \sum_{n=0}^{\infty} a_{n,m} \psi_{n,m}(r) f_n(z) \right), \quad r > R \tag{6.2}$$

with

$$\psi_{n,m}(r) = \begin{cases} H_m^{(1)}(k_0 r) & \text{for } n = 0 \\ \mathcal{K}_m(K_n r) = H_m^{(1)}(\mathrm{i}K_n r) & \text{for } n = 1, 2, \ldots \end{cases} \tag{6.3}$$

where $H_m^{(1)}$ is the first Hankel function of order $m$. The first term in (6.2) corresponds to the incident wave and the series to the scattered/radiated waves. In the circular region of buoys, $0 < r < R$, we can expand the potential as:

$$\bar{\phi}_m = \frac{-\mathrm{i}}{\omega f_0(0)} \sum_{n=0}^{\infty} b_{n,m} \Psi_{n,m}(r) F_n(z), \quad 0 < r < R, \tag{6.4}$$

with

$$\Psi_{n,m}(r) = J_m(K_n r)$$

where $(f_n, k_n)$ and $(F_n, K_n)$ are the same as before. Let us denote the common radial flux along $r = R$ by

$$U_m(\theta, z) = \frac{\partial \bar{\phi}_m}{\partial r}, \quad r = R. \tag{6.5}$$

The expansion coefficients are found in terms of $U_m$ by orthogonality:

$$a_{0,m} = \frac{\langle U_m|f_0\rangle - \varepsilon_m \mathrm{i}^m k_0 J'_m(k_0R)}{\psi'_{0,m}(R)} \tag{6.6}$$

$$a_{n,m} = \frac{\langle U_m|f_n\rangle}{\psi'_{n,m}(R)} \tag{6.7}$$

$$b_{n,m} = \frac{\langle U_m|F_n\rangle}{\Psi'_{n,m}(R)} \tag{6.8}$$

which ensures the continuity of radial flux. Continuity of pressure (i.e. potential) at $r = R$ requires that

$$\varepsilon_m \mathrm{i}^m \left( J_m(k_0R) - \frac{k_0 J'_m(k_0R)}{\psi'_{0,m}(R)} \psi_{0,m}(R) \right) f_0(z) + \sum_{n=0}^{\infty} \frac{(U_m|f_n)}{\psi'_{n,m}(R)} \psi_{n,m}(R) f_n(z) = \sum_{n=0}^{\infty} \frac{\langle U_m|\phi_n\rangle}{\Psi'_{n,m}(R)} \Psi_{n,m}(R) F_n(z) \tag{6.9}$$

Introducing the expansions

$$f_i = \sum_j M_{ij} F_j, \quad U_m = \sum_j U_{j,m} F_j \tag{6.10}$$

We get

$$\left( J_m(k_0R) - \frac{k_0 J'_m(k_0R)}{\psi'_{0,m}(R)} \psi_{0,m}(R) \right) \sum_j M_{0j} F_j(z) + \sum_{i,j,k} \frac{\psi_{k,m}(R)}{\psi'_{k,m}(R)} M_{ki} U_{i,m} M_{kj} F_j(z) = \sum_n \frac{\Psi_{n,m}(R)}{\Psi'_{n,m}(R)} U_{n,m} F_n(z) \tag{6.11}$$

for $m = 0, 1, 2, \ldots$. By taking the scalar product with $F_p$, we finally obtain for any value of $m$

$$\sum_j \left[ \left( \sum_k M_{kp} \frac{\psi_{k,m}(R)}{\psi'_{k,m}(R)} M_{kj} \right) - \frac{\Psi_{p,m}(R)}{\Psi'_{p,m}(R)} \delta_{p,j} \right] U_{j,m} = - \varepsilon_m \mathrm{i}^m \left( J_m(k_0R) - \frac{k_0 J'_m(k_0R)}{\psi'_{0,m}(R)} \psi_{0m}(R) \right) M_{0p} \tag{6.12}$$

which is a matrix equation for the unknown vector $U_{j,m}$ for every $m$. Numerical computations can be carried out after truncation of the series. After solving for $U_{j,m}$, the velocity $U_m$ hence $\overline{\phi}_m$ are found. Combining (6.2) and (3.21), we get the displacement of the buoys

$$\zeta_0(r,\theta) = \mathcal{F}_0(\omega) \sum_{m=0}^{\infty} \sum_{n=0}^{\infty} b_{n,m} \Psi_{n,m}(r) \frac{F_n(0)}{f_0(0)} \cos(m\theta) \tag{6.13}$$

Again it is proportional to the free surface displacement in the same area according to (3.22). Hence we only show in figure 9 the free surface displacement in and outside the buoy area, for two arrays of radii $R = 1$ and $R = 5$. For the smaller array the displacement is relatively uniform and less than 1. For the larger array, the displacement is significantly reduced on the leeward side.

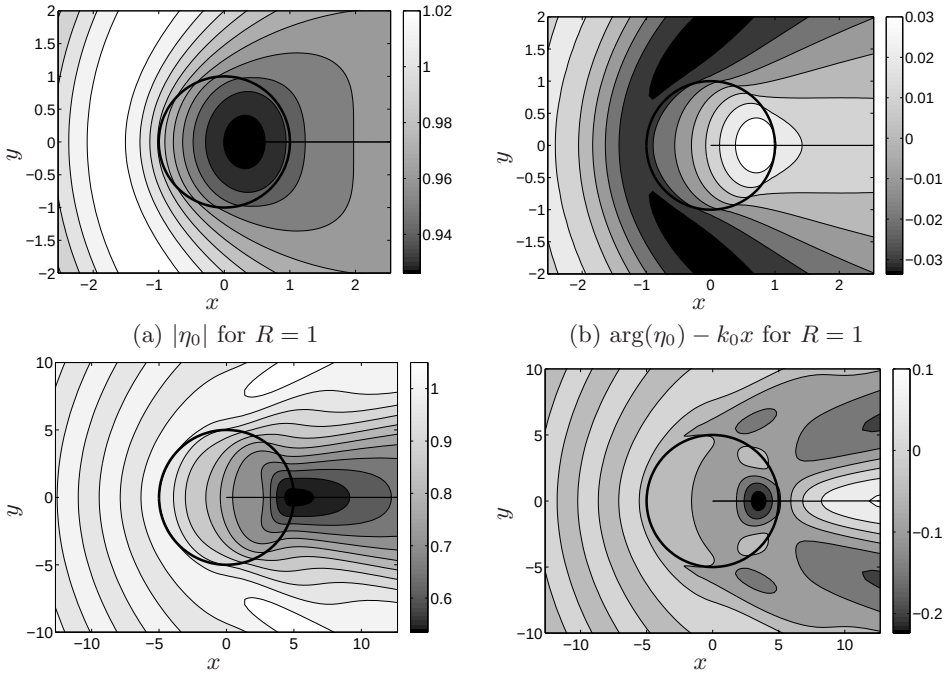


(a) $|\eta_0|$ for $R = 1$ (b) $\arg(\eta_0) - k_0 x$ for $R = 1$

(c) $|\eta_0|$ for $R = 5$ (d) $\arg(\eta_0) - k_0 x$ for $R = 5$

FIGURE 9. Free surface elevation in the neighbourhood of a circular array of buoys. The circumference of the array is represented by the bold circle. $\lambda = 0.5$, $f = 0.2$ and $k_0 = 1$. Waves are incident from the left. Lighter colour corresponds to larger displacement. The phase difference indicated by varying shades of gray is measured in radians.

### 6.2. *Energy absorption*

One can evaluate the extracted energy by calculating the total energy flux into a large circular cylindrical surface of radius $r \gg R$. In physical variables the power output is

$$\begin{aligned}\mathcal{P}^* &= \int_0^{2\pi}\int_{-h^*}^{0} \overline{\left(\mathrm{Re}(\mathrm{i}\rho\omega^*\phi^*)\frac{\partial \mathrm{Re}(\phi^*)}{\partial r^*}\right)} r^*\,\mathrm{d}z^*\,\mathrm{d}\theta \\ &= \rho\sqrt{\frac{g}{h^*}}A^{*2}gh^*h^*\int_0^{2\pi}\int_{-1}^{0}\frac{1}{2}\mathrm{Re}\left(\mathrm{i}\phi\frac{\partial\phi^\dagger}{\partial r}\right) r\,\mathrm{d}z\,\mathrm{d}\theta \end{aligned} \tag{6.14}$$

where the overline denotes time averaging over a period and dagger indicates complex conjugate. Use has been made of the normalization defined in (2.10). The implied normalization for power output is

$$\mathcal{P}^* = \mathcal{P}\left(\rho\sqrt{\frac{g}{h^*}}A^{*2}gh^{*2}\right) \tag{6.15}$$

In contrast, the power flux per unit length of the incoming wave crest is,

$$\frac{1}{2k_0^*}\rho g A^{*2}C_g^* = \frac{1}{2}h^*\rho g A^{*2}\sqrt{\frac{g}{h^*}}h^*\frac{1}{k_0}\frac{d\omega}{dk_0} = \left(\rho g A^{*2}\sqrt{\frac{g}{h^*}}h^{*2}\right)\frac{C_g}{2k_0}$$

where $C_g = C_g^*/\sqrt{gh^*}$ is the dimensionless group velocity of the incoming plane wave. As in early theories the capture width $\mathcal{W}^*$ can be defined as the ratio of the absorption rate to the influx rate of wave power within unit length of the incoming wave front. As a measure of effectiveness, $k_0^*\mathcal{W}^*$ represents the fraction of a wavelength where the

incoming power is depleted,

$$k_0^*\mathcal{W}^* = k_0\mathcal{W} = \frac{\mathcal{P}^*}{\frac{1}{2k_0^*}\rho g {A^*}^2 C_g^*} = \frac{2k_0\mathcal{P}}{C_g} \tag{6.16}$$

Using the asymptotic expansions of Bessel functions for large $k_0 r$, we get from (6.2),

$$\overline{\phi}_m(r) \approx \mathcal{A}_m\sqrt{\frac{2}{\pi k_0 r}}\mathrm{e}^{\mathrm{i}(k_0 r-\pi/4)}\frac{-\mathrm{i}}{\omega f_0(0)}f_0(z) \qquad \text{for } k_0 r \gg 1 \tag{6.17}$$

so that

$$\phi(r) \approx \frac{-\mathrm{i}}{\omega f_0(0)}\left(\mathrm{e}^{\mathrm{i}k_0 r\cos(\theta)} + \sum_m \mathcal{A}_m\sqrt{\frac{2}{\pi k_0 r}}\mathrm{e}^{\mathrm{i}(k_0 r-\pi/4)}\cos(m\theta)\right)f_0(z) \tag{6.18}$$

where the modal amplitudes $\mathcal{A}_m$ can be computed from the solution using the asymptotic expression of the Hankel functions:

$$\mathcal{A}_m = a_{0,m}\mathrm{i}^{-m}$$

Using the method of stationary phase it can be shown that :

$$\mathcal{P} = 2\frac{1}{\omega f_0(0)^2}\left[|\mathcal{A}_0|^2 + \frac{1}{2}\sum_{m\geq 1}|\mathcal{A}_m|^2 + \mathrm{Re}\left(\sum_{m\geq 0}\mathcal{A}_m\right)\right] \tag{6.19}$$

Details are similar to that in Mei *et al.* (2005), p.381, and omitted. The capture width is therefore:

$$k_0^*\mathcal{W}^* = k_0\mathcal{W} = \frac{4k_0}{\omega C_g f_0(0)^2}\left[|\mathcal{A}_0|^2 + \frac{1}{2}\sum_{m\geq 1}|\mathcal{A}_m|^2 + \mathrm{Re}\left(\sum_{m\geq 0}\mathcal{A}_m\right)\right]$$

Finally, using the expression for $f_0$ and the dispersion relation, we find

$$C_g f_0(0)^2 = \frac{k_0}{\omega}$$

hence

$$k_0\mathcal{W} = 4\left(|\mathcal{A}_0|^2 + \frac{1}{2}\sum_{m\geq 1}|\mathcal{A}_m|^2 + \mathrm{Re}(\sum_{m\geq 0}\mathcal{A}_m)\right) \tag{6.20}$$

The same result can also be derived by calculating the rate of work done on the heaving buoys. Another measure of effectiveness is the ratio of the extraction rate to the influx rate across the entire diameter of the array, $\mathcal{W}/2R$ which is expected to be less than unity.

For evaluating the merits of the compact array let us first recall some results known for a single buoy : (i) The optimal $k_0\mathcal{W}$ is 1 at best for a heaving buoy of any size. If all three degrees of freedom are used to extract energy then maximum $k_0\mathcal{W} = 3$ (Newman (1979), Falnes (2002), Mei *et al.* (2005)). (ii) The peak value of $k_0\mathcal{W}$ occurs at $k_0 a_b = O(1)$. In other words, the peak occurs at higher $k_0 = k^*h^*$ for smaller $a_b = a_b^*/h^*$. (iii) The curve of $k_0\mathcal{W}$ versus $k_0 = k^*h^*$ has a broader peak for a smaller $a_b$. Properties (ii) and (iii) are based on numerical computations via the eigenfunction expansion method of Black, Mei & Bray (1971) and are confirmed by approximate reasoning in Appendix B.

In light of these let us present the results for a circular array of buoys. Figure 10 shows the dependence of the two measures of effectiveness on the extraction rate $\lambda$. For

two different array radii $R$, the greatest $k_0\mathcal{W}$ and $\mathcal{W}/2R$ are achieved at around the same extraction rate of $\lambda = 0.5$. The optimal rate of extraction depends slightly on the frequency/wave-number of the incoming wave.

Figure 11 shows that for a fixed packing ratio and damping rate, the capture width $k\mathcal{W}$ and efficiency $\mathcal{W}/2R$ naturally increase with the radius of the array. More important, the bandwidth of both quantities is very large for all array sizes.

Figure 12 shows that the capture width increases monotonically with the packing ratio $f$, and with the incoming wave frequency. Recall that for circular buoys in a square array the maximum packing ratio is $f \leq \pi/4 \approx 0.8$.

Finally let us compare a large buoy whose radius and draft are equal, with a buoy array of the same total displaced volume $\pi f R^2 H$ where $H \equiv H^*/h^*$ and is taken to be $H = 0.1$ for illustration†. Then the radius and draft of the large buoy are both $a_b = (fR^2H)^{1/3}$. Figure 13 compares the capture widths over a wide range of frequencies. The solid curves gives the capture width for an array for different radii $R$, with fixed $f = 0.2$ and $\lambda = 0.5$. The dashed curves represent the capture width for a single-buoy absorber of radius $a_b$. In the range of $0 < k_0(= k_0^* h^*) < 6$ the maximum $k_0\mathcal{W}$ is at most unity for a single heaving buoy, and can be 3 if roll and sway can also be resonated. Note however that the band width of a single buoy is always much narrower. Thus the circular buoy array is potentially more advantageous from the technical viewpoint of efficiency.

## 7. Conclusions

Stimulated by a recent invention in Norway, we have developed a theory for the hydrodynamics and power-extraction efficiency of a compact array of small buoys. The typical wave length is assumed to be comparable to the overall radius of the array but much greater than the dimensions of individual buoys. For a periodic array the two-scale method of homogenization leads to an effective equation governing the spatial average. The energy-absorbing efficiency is studied for a long strip of buoys and for a circular array. The latter geometry is shown to be potentially advantageous, having good efficiency over a broad range of frequencies, unlike that of one large buoy. The theory can be readily modified for wave interaction with broken ice floes on the sea surface, if the ice floes are idealized as identical floating bodies in a periodic array.

Finally, we stress that the homogenization theory employed here is effective only when two sharply different scales exist. When both the buoy dimension and the spacing are not small compared to the wavelength, direct numerical methods are available but require greater computational effort. For simple geometries such as vertical circular cylinders, formally exact theories have been reported by Linton & Evans (1990); Manihar & Newman (1997); Linton & Mclver (1996); Chamberlain (2007); Linton & Evans (1992); Linton & Mclver (1996) for an infinite or semi-infinite line of fixed vertical cylinders with finite radius. These methods still call for significant numerical work. Approximate theories on the interaction of water waves with many floating objects have been given by Falnes (1980); Falnes & Budal (1982); Falnes (1984); de O. Falcao (2002) for large separation and weak hydrodynamic interactions without Bragg scattering. For Bragg scattering by an array of very slender vertical cylinders, the present approximation leads to explicit analytical results and the accuracy has been numerically confirmed by Li & Mei (2007) using the method of finite elements.

We thank Drs. Yuming Liu and Dick Yue of MIT for illuminating discussions. This

† The dimensionless draft $H$ of small buoys does not influence the energy extraction, but a value is chosen here to define the total volume for the array.

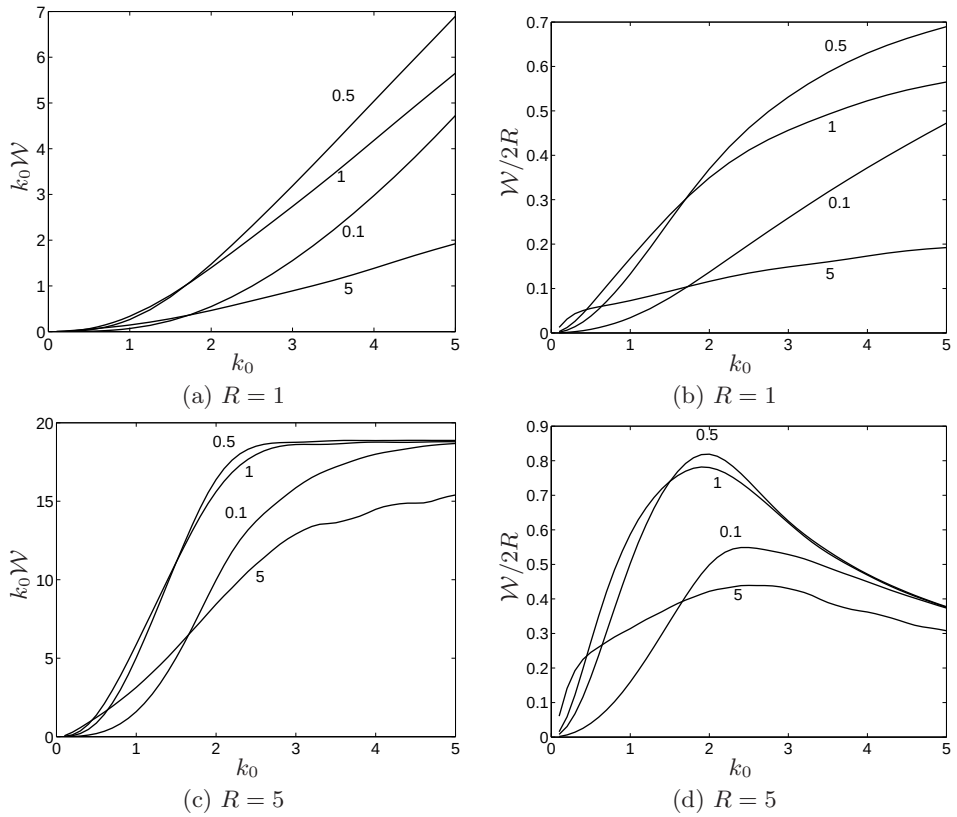


(a) $R = 1$ (b) $R = 1$

(c) $R = 5$ (d) $R = 5$

FIGURE 10. Dependence of effectiveness on the extraction rate $\lambda$ whose values are indicated next to the curves. The packing ratio is $f = 0.2$.

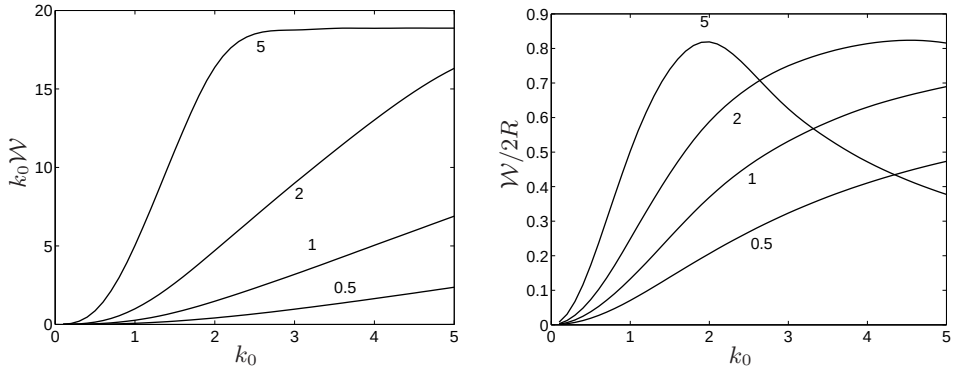


(a) $2\pi\times$Capture width/wavelength (b) Ratio of capture width to array radius.

FIGURE 11. Dependence of the effectiveness on the array radius $R$ whose values are indicated next to the curves. ($\lambda = 0.5$ and $R = 1$).

research has been supported by a grant from MASDAR Institute of Science and Technology in the program of MIT-Abu Dhabi Alliance. Partial support has been received from US-Israel Bi-National Science Foundation and from an ignition grant by MIT Earth System Initiative.

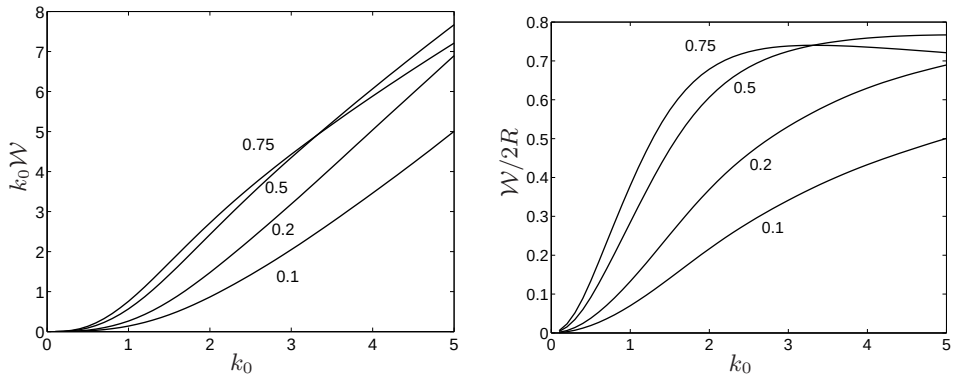


(a) $2\pi\times$Capture width/wavelength (b) Ratio of capture width to array radius.

FIGURE 12. Dependence of effectiveness on the packing ratio $f$ whose values are indicated next to the curves. ($\lambda = 0.5$ and $R = 1$)

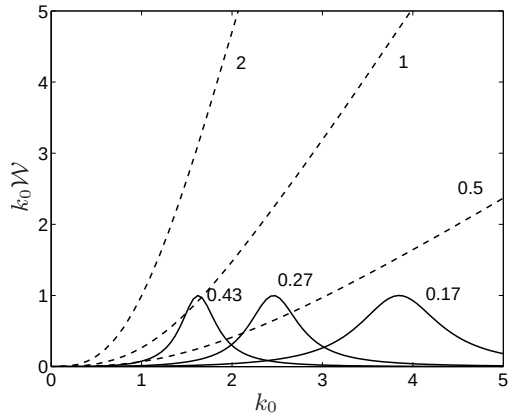


FIGURE 13. Capture widths of a circular arrays of small buoys of radii $R = 0.5, 1, 2$ are shown by dashed curves. Their drafts are $H = H^*/d^* = 1/10$. Capture widths of a large buoy of equal total volume with radii $a_b = (fR^2H)^{\frac{1}{3}} = 0.17, 0.27, 0.43$ are shown by solid curves. The draft is equal to the radius. For the array $f = 0.2$, $\lambda = 0.5$. For the single buoys the extraction rate is chosen to be the maximum at the peak.

## Appendix A. Numerical confirmation of the localization of $N_j(\boldsymbol{x})$

The distributions of the $N_j$ in a cell are computed by the Finite Element Method, and plotted in Figure 14. For $N_3$ the constraint $N_3(0, 0, -1) = 0$ was imposed for uniqueness. It can be seen that all solutions diminish rapidly with the depth.

## Appendix B. Order estimate for a single buoy

When a heaving buoy of radius $a_b$ and draft $H_b$ is at resonance, the buoyancy restoring force $\rho g\pi a_b^2$ roughly equals the total (real and hydrodynamic) inertia $\alpha\rho\pi a_b^2 H$ where $\alpha = O(1)$. Thus the resonance frequency is

$$\omega^{*2} = \frac{\rho g\pi a_b^{*2}}{\alpha\rho\pi a_b^{*2} H_b^*}, \quad \text{or} \quad \omega^2 = \frac{1}{a_b}\frac{a_b}{\alpha H_b} \tag{B 1}$$

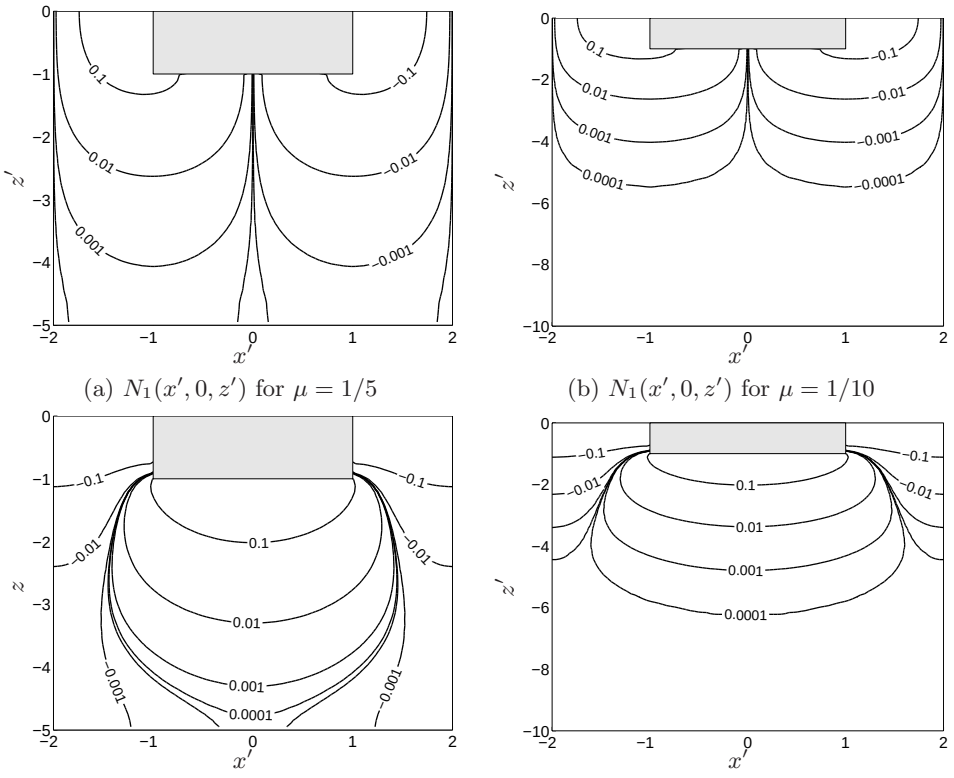


(a) $N_1(x', 0, z')$ for $\mu = 1/5$ (b) $N_1(x', 0, z')$ for $\mu = 1/10$

(c) $N_3(x', 0, z')$ for $\mu = 1/5$ (d) $N_3(x', 0, z')$ for $\mu = 1/10$

FIGURE 14. Finite element solutions of (3.33) and (3.34) for a tall cell with $H' = 1$, $d' = 4$ and different $\mu$. Note the exponential decay with depth.

By the dispersion relation, resonance occurs at

$$k_0 a_b = \frac{a_b}{\alpha H_b \tanh(k_0)} \tag{B 2}$$

For $k_0 = O(1)$ and $a_b/H_b = O(1)$, we get $k_0 a_b = O(1)$ at resonance. In the plot of $k_0\mathcal{W}$ vs $k_0$, resonance is at higher value of $k_0$ if $a_b$ is smaller, as shown in Figure 13.

The dimensionless capture width can be shown to be

$$k_0\mathcal{W} = \frac{k_0}{C_g} \frac{\lambda_g \omega^2 |F_z^D|^2}{\omega^2(\lambda_{zz} + \lambda_g)^2 + (\pi a_b^2 - \omega^2 (\pi a_b^2 H + \mu_{zz}))^2} \tag{B 3}$$

where $F_D$ represents the diffraction force, $\lambda_{zz}$ the radiation damping coefficient (normalized according to $\lambda_{zz} = \lambda^*_{zz}/\rho g^{1/2} h^{*5/2}$) and $\mu_{zz}$ the hydrodynamic mass. Using the fact that the capture width is at its peak value of unity when resonance occurs and $\lambda_g = \lambda_{zz}$, (B 3) can be approximated by

$$k_0\mathcal{W} \approx \frac{(2\lambda_{zz}\omega)^2}{\pi a_b^2(1 - \alpha H \omega^2) + (2\lambda_{zz}\omega)^2} \tag{B 4}$$

around the peak where $1 - \alpha H \omega^2 \approx 0$ and $\alpha = O(1)$ is a constant. The values of $\omega^2 = \omega_\pm^2$ when $k_0\mathcal{W} = 1/2$ on both sides of the peak are found to be

$$\omega_\pm^2 \approx \frac{\pi a_b^2 \pm 2\lambda_{zz}\omega}{\alpha \pi a_b^3} \tag{B 5}$$

hence

$$\omega_+^2 - \omega_-^2 \approx \frac{4\lambda_{zz}\omega}{\alpha\pi a_b^3} \tag{B 6}$$

or

$$k_{0+} - k_{0-} \approx \frac{4\lambda_{zz}\omega}{\alpha\pi a_b^3} \tag{B 7}$$

since $\omega^2 = O(k_0)$. For small $k_0 a_b$ it is known that (Mei *et al.* (2005))

$$\lambda_{zz}^* = \frac{\rho g k_0^* a_b^{*4}}{4C_g^*}$$

Numerical computations show that this order of magnitude is still valid $k_0 a_b = O(1)$, hence

$$\lambda_{zz} = O\left(\frac{k_0 a_b}{C_g} a_b^3\right)$$

Since at the peak $k_0 a_b = O(1)$, which implies $\omega = O(a_b^{-1/2})$ and $C_g = O(a_b^{1/2})$, it follows that

$$\lambda_{zz} = O(a_b^{5/2})$$

Thus the peak width of the $k_0\mathcal{W}$ vs. $k_0$ curve is

$$k_{0+} - k_{0-} \propto a_b^{-1} \tag{B 8}$$

Consequently the peak width is larger for a smaller buoy, as shown in Figure 13.

## REFERENCES


Abramowitz, M. & Stegun, I.A. 1964 *Handbook of mathematical functions.*. Dover Publications.

Black, J.L., Mei, C.C. & Bray, M.C.G. 1971 Radiation and scattering of water waves by rigid bodies. *Journal of Fluid Mechanics* **46** (1), 151–164.

Budal, K. & Falnes, J. 1980 *Power from Sea Waves*, chap. Interacting point absorbers with controlled motion. Academics Press.

Chamberlain, P.G. 2007 Water wave scattering by finite arrays of circular structures. *IMA J Appl Math* **72** (1), 52–66.

Dalrymple, R.A., Losada, M.A. & Martin, P.A. 1991 Reflection and transmission from porous structures under oblique wave attack. *Journal of Fluid Mechanics* **224**, 625–644.

Falnes, J. 1980 Radiation impedance matrix and optimum power absorption for interacting oscillators in surface waves. *Applied Ocean Research* **2** (2), 75–80.

Falnes, J. 1984 Wave-power absorption by an array of attenuators oscillating with unconstrained amplitudes. *Applied Ocean Research* **6** (1), 16–22.

Falnes, J. 2002 *Ocean Waves and Oscillating Systems*. Cambridge University Press.

Falnes, J. & Budal, K. 1982 Wave-power absorption by parallel rows of interacting oscillating bodies. *Applied Ocean Research* **4** (4), 194–207.

Li, Y. & Mei, C.C. 2007 Bragg scattering by a line array of small cylinders in a waveguide. part 1. linear aspects. *Journal of Fluid Mechanics* **583** (-1), 161–187.

Linton, C.M. & Evans, D.V. 1992 The radiation and scattering of surface waves by a vertical circular cylinder in a channel. *Philosophical Transactions: Physical Sciences and Engineering* **338** (1650), 325–357.

Linton, C.M. & Mclver, R. 1996 The scattering of water waves by an array of circular cylinders in a channel. *Journal of Engineering Mathematics* **30** (-1), 661–682.

Linton, C. M. & Evans, D. V. 1990 The interaction of waves with arrays of vertical cylinders. *Journal of Fluid Mechanics* **215**, 549–569.

Manihar, H. D. & Newman, J. N. 1997 Wave diffraction by a long array of cylinders. *Journal of Fluid Mechanics* **339**, 309–330.

McIver, P. 1998 The dispersion relation and eigenvalue expansion for water waves in porous structures. *Journal of Engineering Mathematics* **34**, 319–334.

Mei, C.C., Stiassnie, M. & Yue, D.K.P 2005 *Theory and application of ocean surface waves.*. World Scientific.

Mynett, A.E., Serman, D.D. & Mei, C.C. 1979 Characteristics of Salter's cam for extracting energy from ocean waves. *Applied Ocean Research* **1**, 13–20.

Newman, J.N. 1979 Absorption of wave energy by elongated bodies. *Applied Ocean Research* **1**, 189–196.

de O. Falcão, A.F. 2002 Wave-power absorption by a periodic linear array of oscillating water columns. *Ocean Engineering* **29** (4), 1164–1186.